Supporting Information for

Anion-doping Optimizes Metal Bonds for Promoting Hydrogen Evolution Performance of NiMoN Catalysts

Minghui Xing[1#], Shaoke Zhu[1#], Guoqing Xu[1], Mengting Han[1], Zhiping Liu[1]*, Qinglan Zhao[2], Minhua Shao[2], Dapeng Cao*[1]

[1] *State Key Laboratory of Organic-Inorganic Composites, Beijing University of Chemical Technology, Beijing 100029, China.*

[2] *Department of Chemical and Biological Engineering, Hong Kong University of Science and Technology, Clear Water Bay, Kowloon, Hong Kong, China*

*Corresponding authors. Email: liuzhp@mail.buct.edu.cn or caodp@mail.buct.edu.cn

Chemicals

nickel (II) nitrate hexahydrate ($Ni(NO_3)_2 \cdot 6H_2O$, AR), Ammonium molybdate tetrahydrate ($(NH_4)_6Mo_7O_{24}\cdot 4H_2O$, AR), sodium chloride (NaCl, 99%), ammonium fluoride (NH_4F, 99.5%), Urea (CH_4N_2O, 99%), Ni foam (NF) (2*4 cm^2) was pretreated in 3 M HCl by ultrasonic treatment for 20 min.

Preparation of Cl-$NiMoO_4$

$Ni(NO_3)_2\cdot 6H_2O$ (348.95 mg), $(NH_4)_6Mo_7O_{24}\cdot 4H_2O$ (370.75 mg) and NaCl (438.75 mg) were dissolved in 30 mL of water. After that, a piece of Ni foam (2*4 cm^2) was placed in above precursor solution in a teflon-lined autoclave (50 mL), followed by heating the solution at 150 °C for 2 h. The as-prepared catalyst was washed with water and dried under Ar. For the sake of overall simplicity of the manuscript, we named it as "Cl-$NiMoO_4$".

Preparation of Cl-NiMoN

For preparing Cl-NiMoN, the Cl-$NiMoO_4$ (2*4 cm^2) was put in the tubular furnace was heated to 500 °C with a heating rate of 5 °C min^{-1} and maintained for 2 h under an NH_3 flow.

Preparation of F-NiMoN, CO_3-NiMoN and F, CO_3-NiMoN

In order to study the effect of different anions on NiMoN. F-NiMoN, CO_3-NiMoN and F, CO_3-NiMoN were also prepared. In the process of synthesizing the R-$NiMoO_4$, instead of NaCl, F-$NiMoO_4$ requires the addition of 148 mg of NH_4F, CO_3-$NiMoO_4$ adds 450 mg of urea as the CO_3^{2-} source. Accordingly, the synthesis of F, CO_3-NiMoN,148 mg NH4F and 450 mg urea were both added. The conditions of

F-NiMoN, Co_3-NiMoN and F, CO_3-NiMoN vapor deposition were the same as Cl-NiMoN.

Characterizations

Powder X-ray diffraction (XRD) data was measured on a RigakuD/MAX 2550 diffractometer with Cu Kα radiation (λ = 1.5418 Å). ZEISS GeminiSEM 300 was used to acquire scanning electron microscopy (SEM) at an accelerating voltage of 3 kV. A ThermoFisherESCALab 250 (ThermoFisher, E. Grinstead, UK) was performed to get the X-ray photoelectron spectroscopy (XPS) data, using Al Ka X-ray radiation for excitation. Energy dispersive X-ray spectroscopy (EDX) and high-resolution TEM (HRTEM) images were obtained by a JEOL JEN-F200 at an accelerating voltage of 200 kV. Inductively coupled plasma optical emission spectroscopy (ICP-OES) was used to confirm the compositions of the samples.

Electrochemical measurements

All the HER catalytic measurements were performed with a CHI 760E electrochemistry workstation (CH Instruments, Inc., Shanghai) in a standard three-electrode system using Cl-NiMoN as the working electrode, a graphite rod as the counter electrode and an Ag/AgCl electrode as the reference electrode. All potentials reported were calibrated to reversible hydrogen electrode (RHE) by E(RHE) =E(Ag/AgCl) + 0.197 V + 0.059 × pH. As show in Figure S8, the zero point of RHE was further calibrated by using the HER/HOR equilibrium potential of Pt catalyst in H_2-saturated solutions ($E_{RHE}=E_{Ag/AgCl}+1.017 \approx E_{Ag/AgCl}+1.02$). Linear sweep voltammetry (LSV) is recorded at a scan rate of 5 mV s^{-1}. Without explanation all

polarization curves are 85% iR corrected by default. The double-layer capacitance (C_{dl}) via cyclic voltammograms (CV) at different scan rates were measured to investigated electrochemically active surface areas (ECSA).

The electrochemically active surface area (ECSA) values were estimated by the electrochemical double layer capacitance (C_{dl}) determined by cyclic voltammetry (CV) curves performed in the non-Faradaic regions at different scan rates. By plotting the difference between the anodic and cathodic current densities ($\Delta j = j_a - j_c$) at the half potential of the CV measurement against the scan rates, the obtained linear slope is the twice of the C_{dl}. The ECSA was calculated by $ECSA = C_{dl}/C_s$.

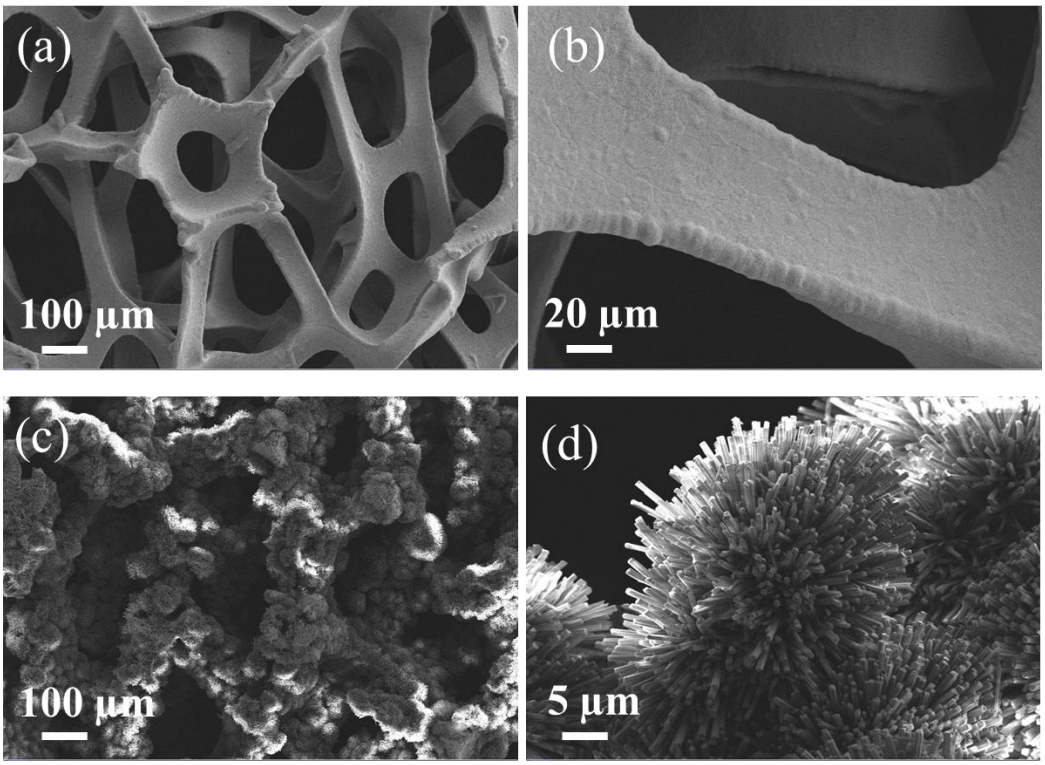

Figure S1. SEM images of (a-b) NF and (c-d) Cl-$NiMoO_4$.

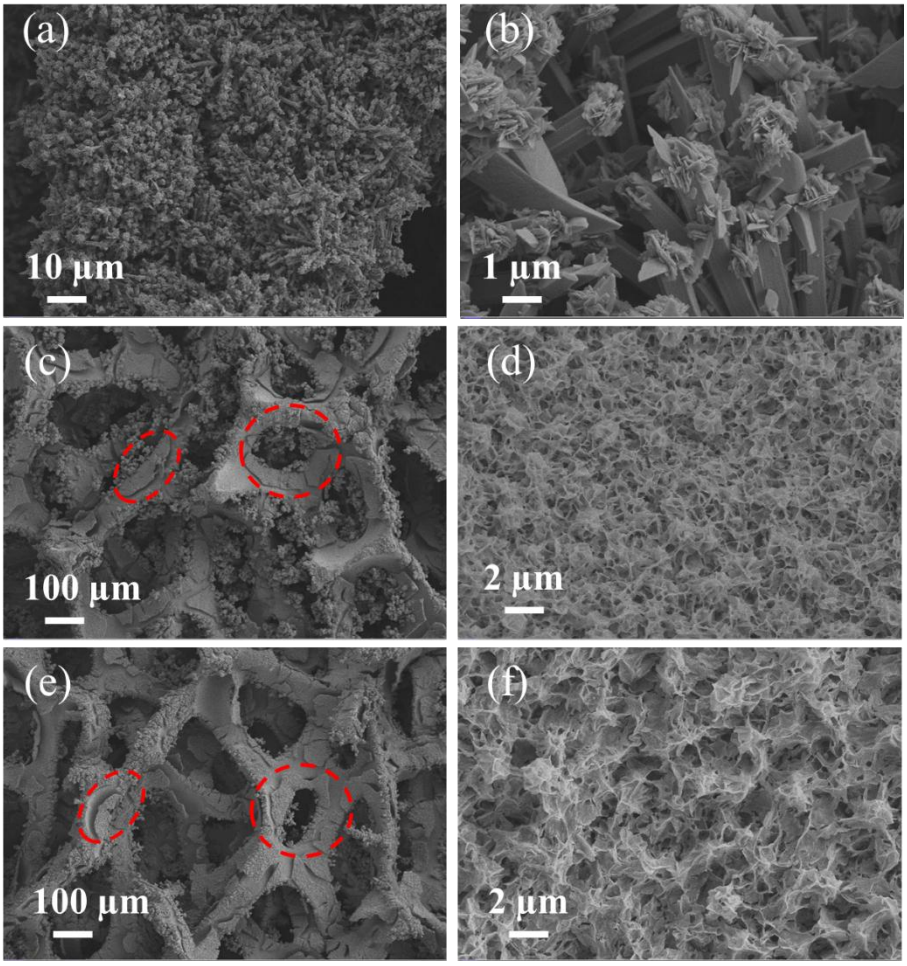

Figure S2. SEM images of (a-b) F-NiMoN, (c-d) CO_3-NiMoN, and (e-f) F, CO_3-NiMoN.

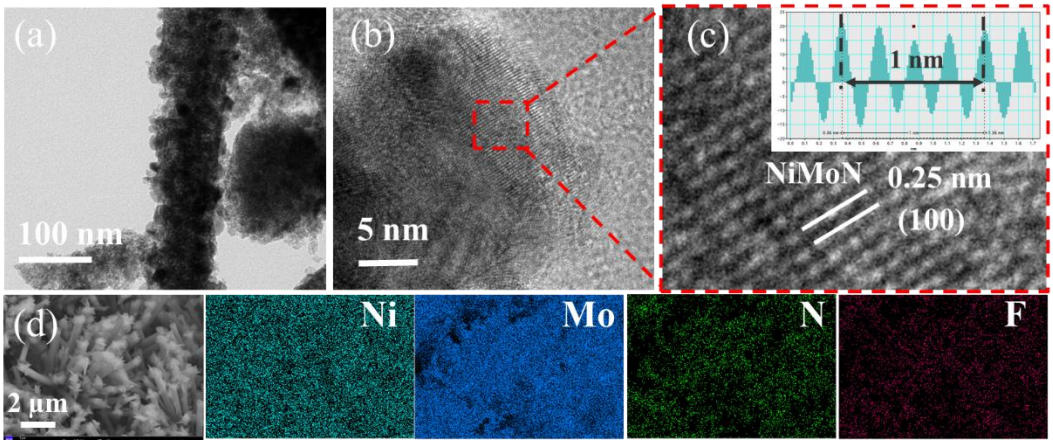

Figure S3. (a) TEM and (b-c) HRTEM images of F-NiMoN. (d) EDS element mappings of Ni, Mo, N and F in F-NiMoN.

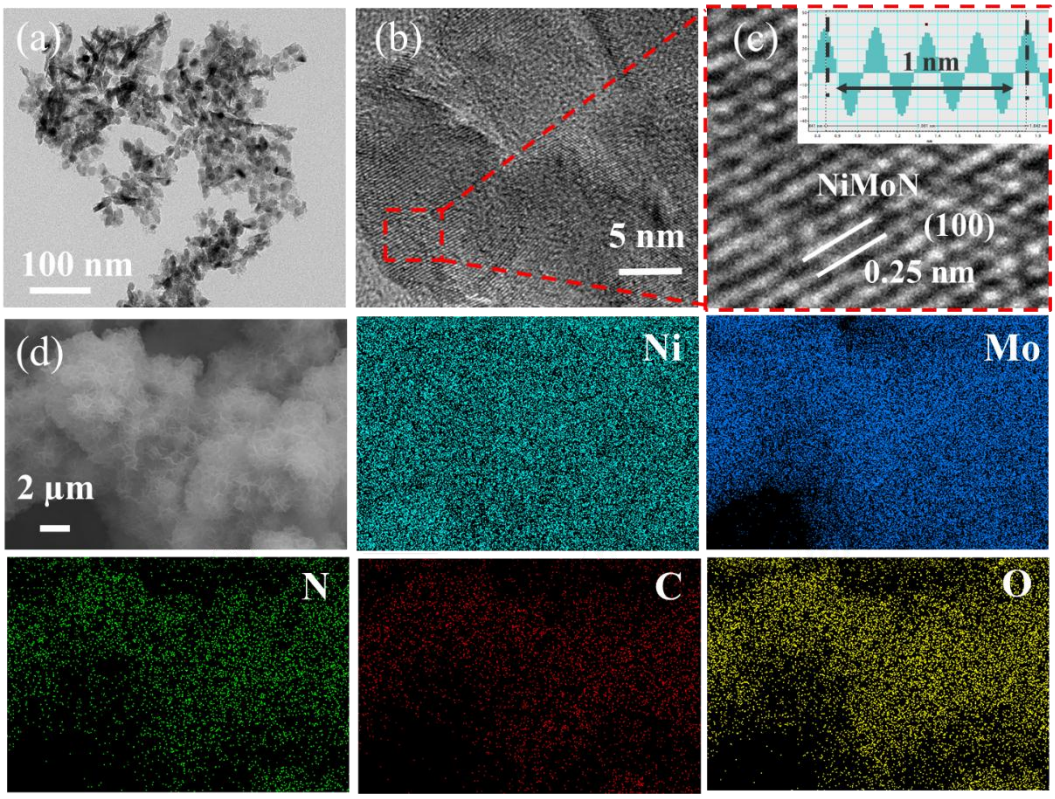

Figure S4. (a) TEM and (b-c) HRTEM images of CO_3-NiMoN. (d) EDS element mappings of Ni, Mo, N, C and O in CO_3-NiMoN.

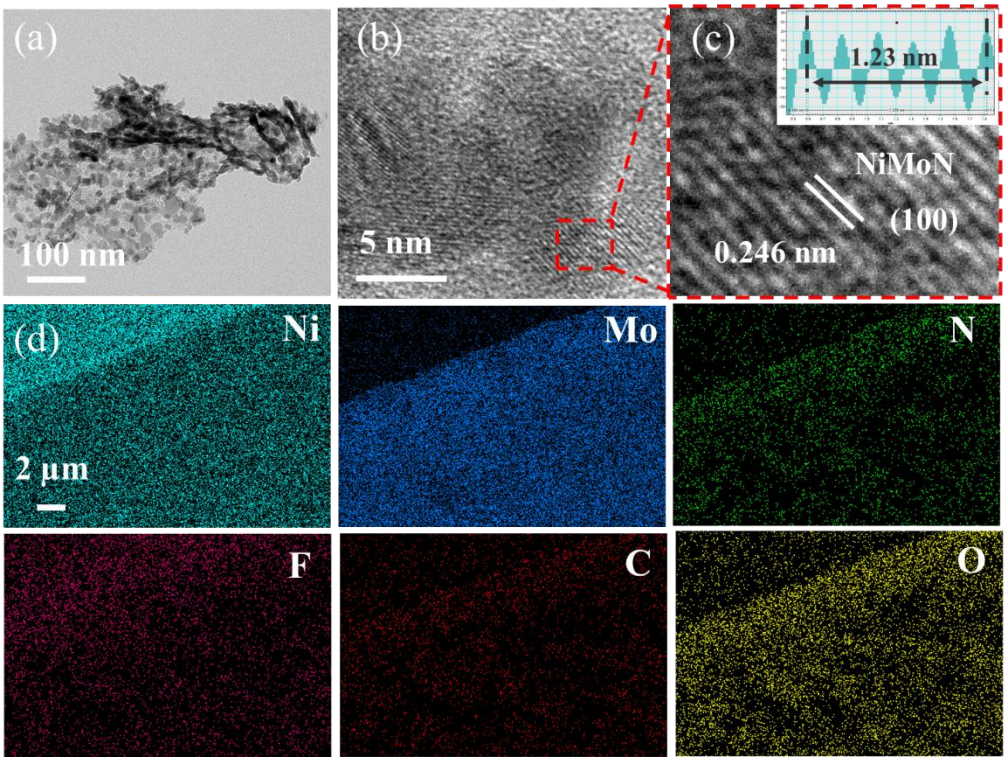

Figure S5. (a) TEM and (b-c) HRTEM images of F, CO_3-NiMoN. (d) EDS element mappings of Ni, Mo, N, F, C and O in F, CO_3-NiMoN.

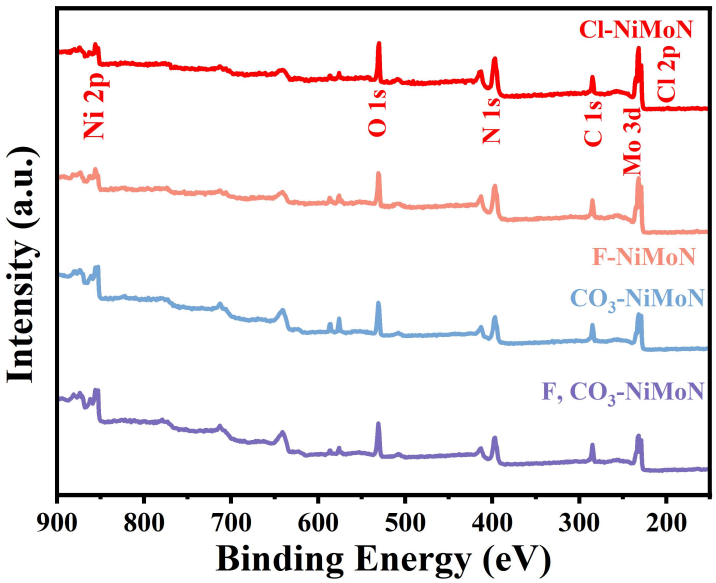

Figure S6. XPS survey spectra of Cl-NiMoN, F-NiMoN, CO_3-NiMoN and F, CO_3-NiMoN.

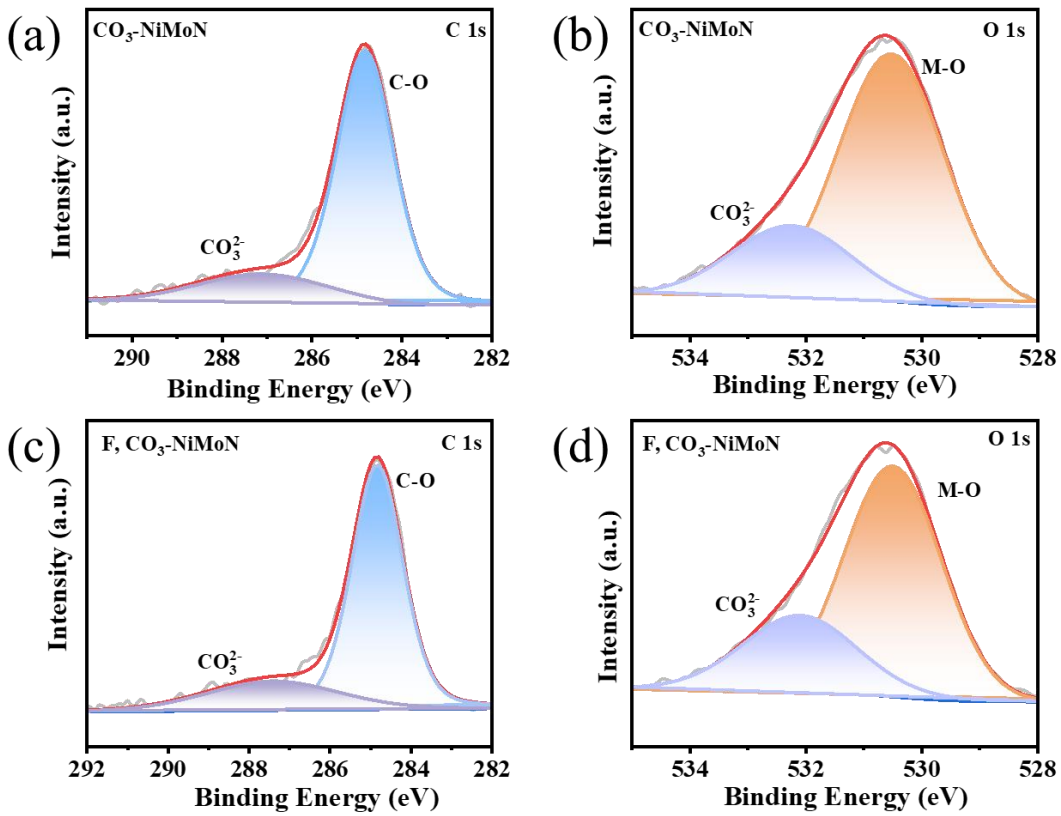

Figure S7. CO_3-NiMoN of (a) C 1s and (b) O 1s. F, CO_3-NiMoN of (c) C 1s and (d) O 1s.

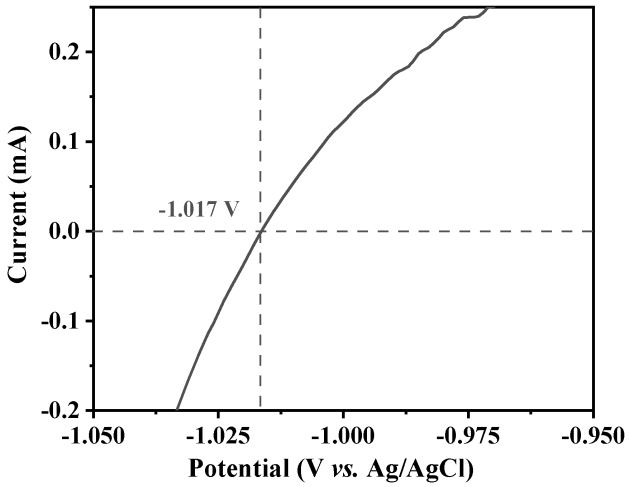

Figure S8. Current-potential curve of Pt wire in highly pure H_2-saturated 1 M KOH aqueous solution, used for calibration of the Ag/AgCl electrode with respect to RHE. Scan rate 1 mV s^{-1}. The potentials were calibrated to $E_{RHE}=E_{Ag/AgCl}+1.017\approx E_{Ag/AgCl}+1.02$.

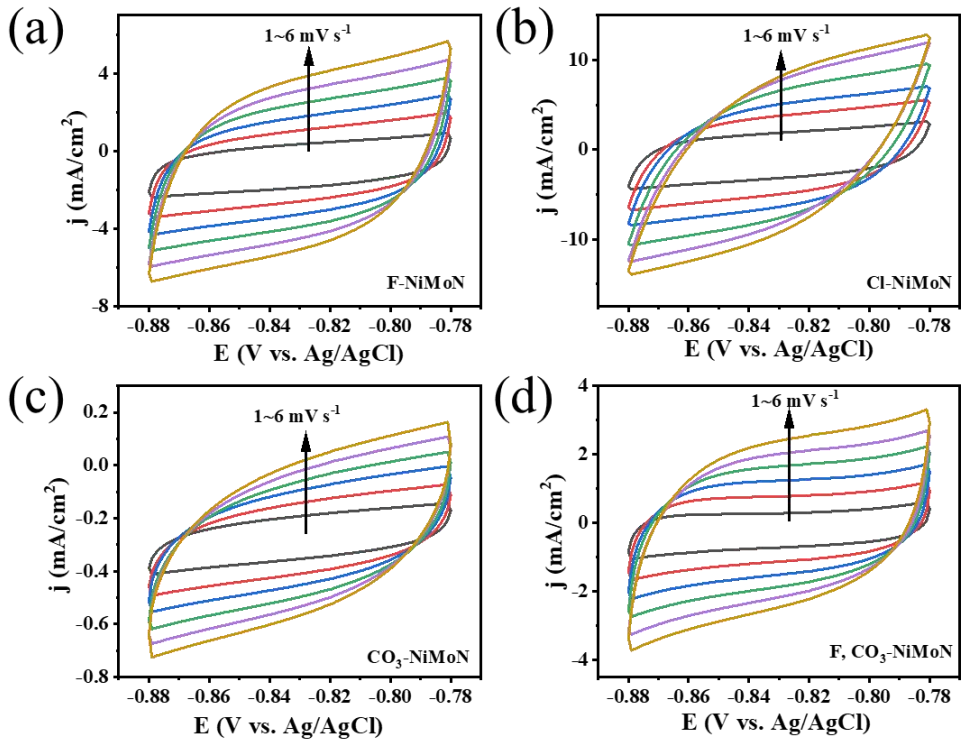

Figure S9. CV plot at different scan rate of Cl-NiMoN, F-NiMoN, CO_3-NiMoN and F, CO_3-NiMoN in 1 M KOH.

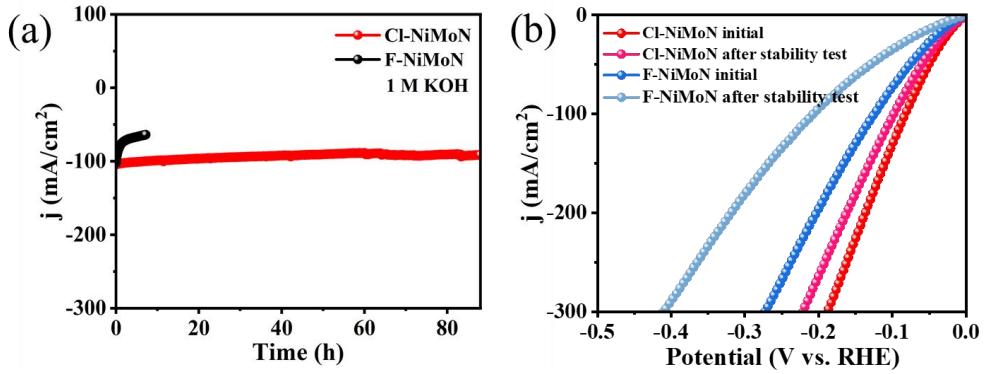

Figure S10. a) Chronoamperometric measurement for Cl-NiMoN and F-NiMoN. b) The LSV curves of Cl-NiMoN and F-NiMoN before and after stability test.

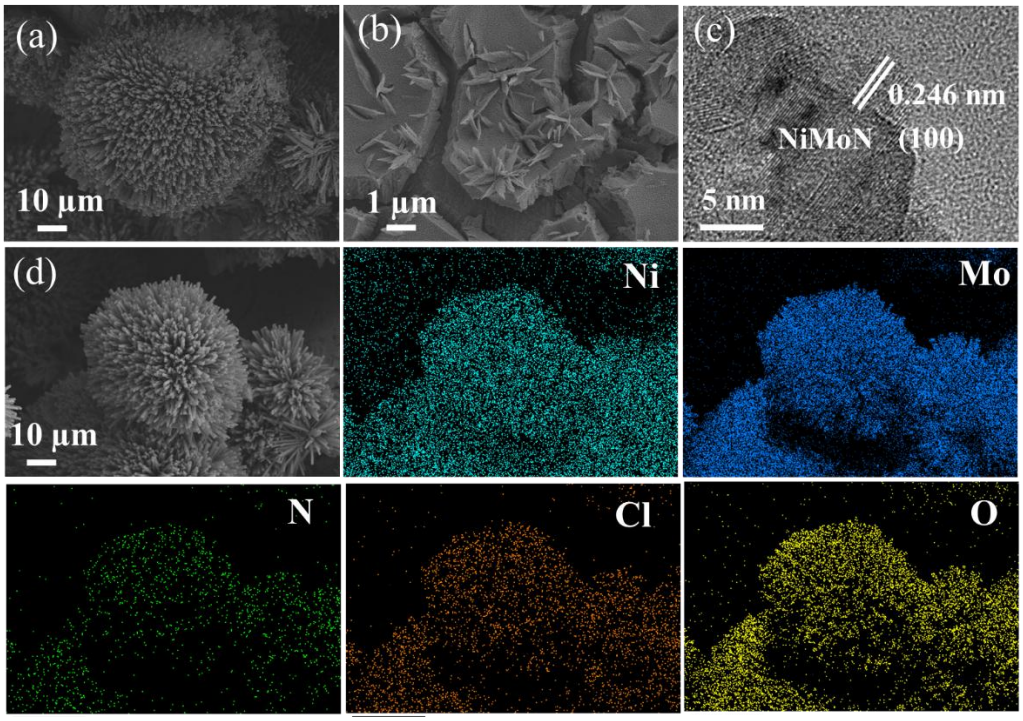

Figure S11. The SEM, TEM images and STEM-EDS mappings of Cl-NiMoN after stability test in 1 M KOH.

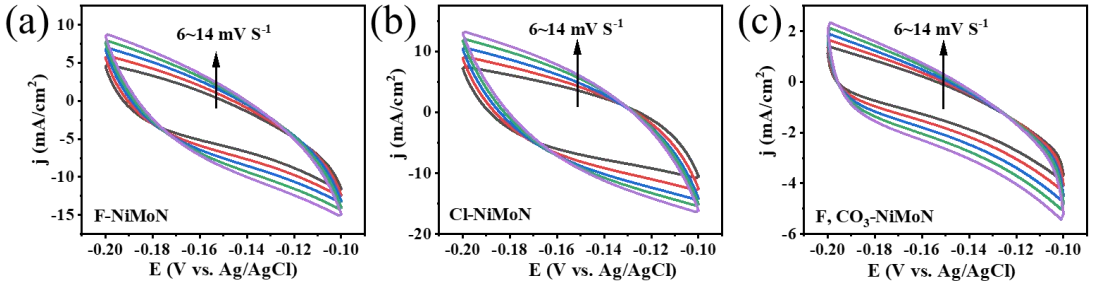

Figure S12. CV plot at different scan rate of Cl-NiMoN, F-NiMoN, and F, CO_3-NiMoN in 0.5 M H_2SO_4.

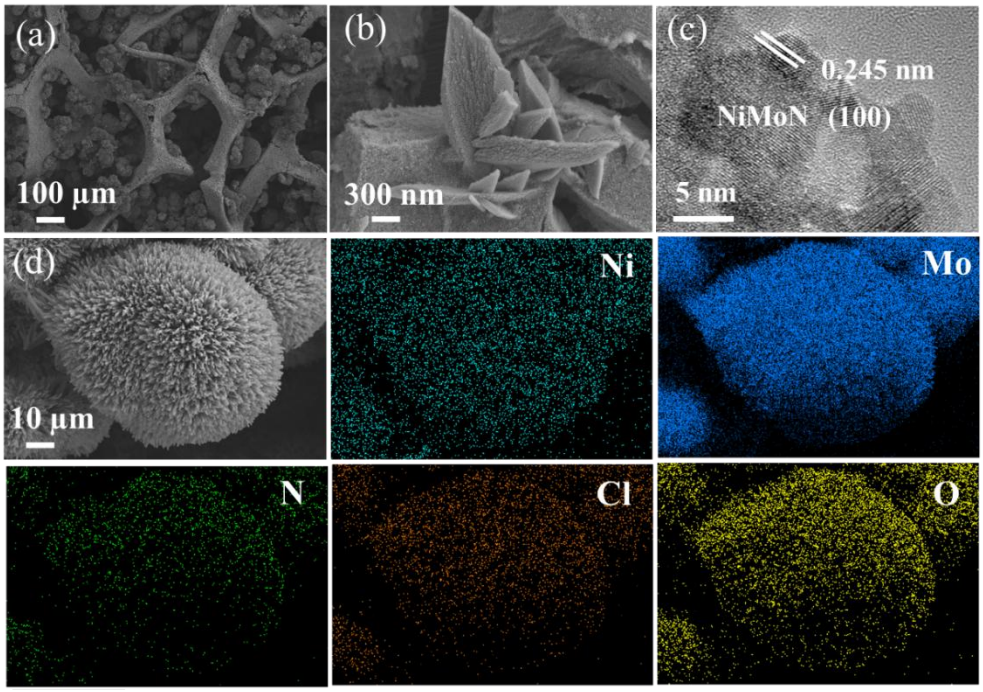

Figure S13. The SEM, TEM images and STEM-EDS mappings of Cl-NiMoN after stability test in 0.5 M H_2SO_4.

Table S1. Comparison of the performance of metal electrocatalysts in alkaline media (η_{10} indicates the overpotential at current density of 10 mA cm^{-2}).

Electrocatalyst	η_{10} (mV)	Tafel slope (mV dec^{-1})	Electrolyte	Reference
Cl-NiMoN	19	32.1	1 M KOH	This work
$Co(OH)_x$@CoP	100	76	1 M KOH	[1]
Rh_2Sb NBs/C	39.5@10	40.1	1 M KOH	[2]
MnCoP/NiP/NF	119.0 (η_{50})	61	1 M KOH	[3]
RuO_2-WC NPs	58@10	66	1 M KOH	[4]
CoP/NPC/TF	80	50	1 M KOH	[5]
Co_3O_4/MoS_2	205	128	1 M KOH	[6]
Ni_2P@NC/NF	84	106	1 M KOH	[7]
$Rh(OH)_3$/CoP	13@10	24	1 M KOH	[8]
CoTeNR/NF	202	115	1 M KOH	[9]
MoS_2/MoP/NC	151	58	1 M KOH	[10]
NiFeRu-LDH	29@10	31	1 M KOH	[11]
Sandwich-like $Co(S_{0.72}Se_{0.28})_2$	106	62	1 M KOH	[12]
Sandwich-like $Co(Te_{0.33}Se_{0.67})_2$	199	131	1 M KOH	[12]
CoS_2–MoS_2	123	86	1 M KOH	[13]
Co–MoS_2/Mo_2CT_x	112	82	1 M KOH	[14]
P-Ru-CoNi-LDH	29@10	69	1 M KOH	[15]
Ni_2P–Co_2P	93	65	1 M KOH	[16]
Mo_2N@NC	85	54	1 M KOH	[17]
Co/CoP@HOMC	120	78	1 M KOH	[18]
Co_2C	73	135	1 M KOH	[19]

Table S2. Comparison of the performance of metal electrocatalysts in acidic media (η_{10} indicates the overpotential at current density of 10 mA cm^{-2}).

Electrocatalyst	η_{10} (mV)	Tafel slope (mV dec^{-1})	Electrolyte	Reference
Cl-NiMoN	22	59.8	0.5 M H_2SO_4	This work
Co_2P/CoN-in-NCNT	98	57	0.5 M H_2SO_4	[20]
Ru@Ni-MOF	112@10	33	0.5 M H_2SO_4	[21]
NiCo-SAD-NC	54.7	31.5	0.5 M H_2SO_4	[22]
$NiCo_2P_x$	104	59.6	0.5 M H_2SO_4	[23]
Co-P-B/CP	172	68	0.5 M H_2SO_4	[24]
CoP/Co_2P/Co	160	56	0.5 M H_2SO_4	[25]
CoP/NPC/TF	91	54	0.5 M H_2SO_4	[5]
PdP_2@CB	30.1@10	29.5	0.5 M H_2SO_4	[26]
CoNiP@NF	155	115	0.5 M H_2SO_4	[27]
Ni_2P–Co_2P	172	67	0.5 M H_2SO_4	[16]
Co_{50}-Mo_2C	125	70.95	1 M $HClO_4$	[28]
Co@NPC	215	70	0.5 M H_2SO_4	[29]
Co/NCNT/NG	123	67	0.5 M H_2SO_4	[30]
Co-SAC/RuO_2	45	58	0.5 M H_2SO_4	[31]
MoS_2/MoP/NC	208	62	0.5 M H_2SO_4	[10]
RuO_2-WC	58	66	0.5 M H_2SO_4	[4]
Ni_2P@NC/NF	68	64	0.5 M H_2SO_4	[7]
PtRu alloy	28@10	33.5	0.5 M H_2SO_4	[32]

[1] L. Su, X. Cui, T. He, L. Zeng, H. Tian, Y. Song, K. Qi, B.Y. Xia, Surface reconstruction of cobalt phosphide nanosheets by electrochemical activation for enhanced hydrogen evolution in alkaline solution, Chem Sci, 10 (2019) 2019-2024.
[2] Y. Zhang, G. Li, Z. Zhao, L. Han, Y. Feng, S. Liu, B. Xu, H. Liao, G. Lu, H.L. Xin, X. Huang, Atomically Isolated Rh sites within highly branched Rh_2Sb nanostructures enhance bifunctional hydrogen electrocatalysis, Adv Mater, 33 (2021) 2105049.
[3] Y. Du, W. Wang, H. Zhao, Y. Liu, S. Li, L. Wang, B. Liu, Ni_2P interlayer and Mn doping synergistically expedite the hydrogen evolution reaction kinetics of Co_2P, Chemistry, 27 (2021) 3536-3541.
[4] S. Sun, H. Jiang, Z. Chen, Q. Chen, M. Ma, L. Zhen, B. Song, C. Xu, Bifunctional WC-supported RuO_2 nanoparticles for robust water splitting in acidic media, Angew Chem Int Ed Engl, (2022) 202202519.
[5] X.K. Huang, X.P. Xu, C. Li, D.F. Wu, D.J. Cheng, D.P. Cao, Vertical CoP nanoarray wrapped by N,P-doped carbon for hydrogen evolution reaction in both acidic and alkaline conditions, Advanced Energy Materials, 9 (2019) 1803970.
[6] A. Muthurasu, V. Maruthapandian, H.Y. Kim, Metal-organic framework derived Co_3O_4/MoS_2 heterostructure for efficient bifunctional electrocatalysts for oxygen evolution reaction and hydrogen evolution reaction, Applied Catalysis B-Environmental, 248 (2019) 202-210.
[7] X. Lv, Z. Hu, L. Chen, J. Ren, Y. Liu, Z. Yuan, Organic–inorganic metal phosphonate-derived nitrogen-doped core–shell Ni_2P nanoparticles supported on Ni foam for efficient hydrogen evolution reaction at all pH values, ACS Sustainable Chemistry & Engineering, 7 (2019) 12770-12778.
[8] M. Xing, S. Zhu, X. Zeng, S. Wang, Z. Liu, D. Cao, Amorphous/Crystalline $Rh(OH)_3$/CoP Heterostructure with Hydrophilicity/Aerophobicity Feature for All‐pH Hydrogen Evolution Reactions, Advanced Energy Materials, 13 (2023) 2302376.
[9] L. Yang, H.X. Xu, H.B. Liu, D.J. Cheng, D.P. Cao, Active site identification and evaluation criteria of in situ grown CoTe and NiTe nanoarrays for hydrogen evolution and oxygen evolution reactions, Small Methods, 3 (2019) 1900113.
[10] J.-Q. Chi, Y.-M. Chai, X. Shang, B. Dong, C.-G. Liu, W. Zhang, Z. Jin, Heterointerface engineering of trilayer-shelled ultrathin MoS_2/MoP/N-doped carbon hollow nanobubbles for efficient hydrogen evolution, Journal of Materials Chemistry A, 6 (2018) 24783-24792.
[11] G. Chen, T. Wang, J. Zhang, P. Liu, H. Sun, X. Zhuang, M. Chen, X. Feng, Accelerated hydrogen evolution kinetics on NiFe-layered double hydroxide electrocatalysts by tailoring water dissociation active sites, Adv Mater, 30 (2018) 1706279.
[12] Y. Wang, L. Liu, Y. Wang, L. Fang, F. Wan, H. Zhang, Constituent-tunable ternary $CoM_{2x}Se_{2(1-x)}$ (M = Te, S) sandwich-like graphitized carbon-based composites as highly efficient electrocatalysts for water splitting, Nanoscale, 11 (2019) 6108-6119.
[13] Y. Wang, Y. Zhu, S. Afshar, M.W. Woo, J. Tang, T. Williams, B. Kong, D. Zhao, H. Wang, C. Selomulya, One-dimensional CoS_2-MoS_2 nano-flakes decorated MoO_2 sub-micro-wires for synergistically enhanced hydrogen evolution, Nanoscale, 11 (2019) 3500-3505.
[14] J. Liang, C. Ding, J. Liu, T. Chen, W. Peng, Y. Li, F. Zhang, X. Fan, Heterostructure engineering of Co-doped MoS_2 coupled with Mo_2CT_x MXene for enhanced hydrogen evolution in alkaline media, Nanoscale, 11 (2019) 10992-11000.
[15] Q. Li, F. Huang, S. Li, H. Zhang, X.Y. Yu, Oxygen vacancy engineering synergistic with surface hydrophilicity modification of hollow Ru doped CoNi-LDH nanotube arrays for boosting hydrogen

evolution, Small, 18 (2022) 2104323.
[16] Q. Cao, S. Hao, Y. Wu, K. Pei, W. You, R. Che, Interfacial charge redistribution in interconnected network of Ni_2P–Co_2P boosting electrocatalytic hydrogen evolution in both acidic and alkaline conditions, Chemical Engineering Journal, 424 (2021) 130444.
[17] Z. Lv, M. Tahir, X. Lang, G. Yuan, L. Pan, X. Zhang, J.-J. Zou, Well-dispersed molybdenum nitrides on a nitrogen-doped carbon matrix for highly efficient hydrogen evolution in alkaline media, J. Mater. Chem. A, 5 (2017) 20932-20937.
[18] W. Li, J. Liu, P.F. Guo, H.Z. Li, B. Fei, Y.H. Guo, H.G. Pan, D.L. Sun, F. Fang, R.B. Wu, Co/CoP Heterojunction on Hierarchically Ordered Porous Carbon as a Highly Efficient Electrocatalyst for Hydrogen and Oxygen Evolution, Advanced Energy Materials, 11 (2021) 2102134.
[19] Y. Qie, Y. Liu, F. Kong, Z. Yang, H. Yang, High coercivity cobalt carbide nanoparticles as electrocatalysts for hydrogen evolution reaction, Nano Research, (2022) 1-6.
[20] Y.Y. Guo, P.F. Yuan, J.A. Zhang, H.C. Xia, F.Y. Cheng, M.F. Zhou, J. Li, Y.Y. Qiao, S.C. Mu, Q. Xu, Co_2P-CoN Double Active Centers Confined in N-Doped Carbon Nanotube: Heterostructural Engineering for Trifunctional Catalysis toward HER, ORR, OER, and Zn-Air Batteries Driven Water Splitting, Advanced Functional Materials, 28 (2018) 1805641.
[21] L. Deng, F. Hu, M. Ma, S.C. Huang, Y. Xiong, H.Y. Chen, L. Li, S. Peng, Electronic modulation caused by interfacial Ni-O-M (M=Ru, Ir, Pd) bonding for accelerating hydrogen evolution kinetics, Angew Chem Int Ed Engl, 60 (2021) 22276-22282.
[22] A. Kumar, V.Q. Bui, J. Lee, L. Wang, A.R. Jadhav, X. Liu, X. Shao, Y. Liu, J. Yu, Y. Hwang, H.T.D. Bui, S. Ajmal, M.G. Kim, S.G. Kim, G.S. Park, Y. Kawazoe, H. Lee, Moving beyond bimetallic-alloy to single-atom dimer atomic-interface for all-pH hydrogen evolution, Nat Commun, 12 (2021) 6766.
[23] R. Zhang, X. Wang, S. Yu, T. Wen, X. Zhu, F. Yang, X. Sun, X. Wang, W. Hu, Ternary $NiCo_2P_x$ Nanowires as pH-Universal Electrocatalysts for Highly Efficient Hydrogen Evolution Reaction, Adv Mater, 29 (2017) 1605502.
[24] J. Kim, H. Kim, S. Kim, S.H. Ahn, Electrodeposited amorphous Co–P–B ternary catalyst for hydrogen evolution reaction, Journal of Materials Chemistry A, 6 (2018) 6282-6288.
[25] A. Sumboja, T. An, H.Y. Goh, M. Lubke, D.P. Howard, Y. Xu, A.D. Handoko, Y. Zong, Z. Liu, One-Step Facile Synthesis of Cobalt Phosphides for Hydrogen Evolution Reaction Catalysts in Acidic and Alkaline Medium, ACS Appl Mater Interfaces, 10 (2018) 15673-15680.
[26] F. Luo, Q. Zhang, X. Yu, S. Xiao, Y. Ling, H. Hu, L. Guo, Z. Yang, L. Huang, W. Cai, H. Cheng, Palladium phosphide as a stable and efficient electrocatalyst for overall water splitting, Angew Chem Int Ed Engl, 57 (2018) 14862-14867.
[27] A. Han, H. Chen, H. Zhang, Z. Sun, P. Du, Ternary metal phosphide nanosheets as a highly efficient electrocatalyst for water reduction to hydrogen over a wide pH range from 0 to 14, Journal of Materials Chemistry A, 4 (2016) 10195-10202.
[28] Y. Ma, M. Chen, H. Geng, H. Dong, P. Wu, X. Li, G. Guan, T. Wang, Synergistically Tuning Electronic Structure of Porous β‐Mo_2C Spheres by Co Doping and Mo‐Vacancies Defect Engineering for Optimizing Hydrogen Evolution Reaction Activity, Advanced Functional Materials, 30 (2020) 2000561.
[29] D. Li, Y. Huang, Z. Li, L. Zhong, C. Liu, X. Peng, Deep eutectic solvents derived carbon-based efficient electrocatalyst for boosting H_2 production coupled with glucose oxidation, Chemical Engineering Journal, 430 (2022).

[30] L. Yang, Y. Lv, D. Cao, Co,N-codoped nanotube/graphene 1D/2D heterostructure for efficient oxygen reduction and hydrogen evolution reactions, Journal of Materials Chemistry A, 6 (2018) 3926-3932.
[31] K. Shah, R. Dai, M. Mateen, Z. Hassan, Z. Zhuang, C. Liu, M. Israr, W.C. Cheong, B. Hu, R. Tu, C. Zhang, X. Chen, Q. Peng, C. Chen, Y. Li, Cobalt Single Atom Incorporated in Ruthenium Oxide Sphere: A Robust Bifunctional Electrocatalyst for HER and OER, Angew Chem Int Ed Engl, 61 (2022) e202114951.
[32] B. Pang, X. Liu, T. Liu, T. Chen, X. Shen, W. Zhang, S. Wang, T. Liu, D. Liu, T. Ding, Z. Liao, Y. Li, C. Liang, T. Yao, Laser-assisted high-performance PtRu alloy for pH-universal hydrogen evolution, Energy & Environmental Science, 15 (2022) 102-108.